One-Step Overall Water Splitting under Visible Light Using Multiband InGaN/GaN Nanowire Heterostructures

Md G. Kibria,[†] Hieu P. T. Nguyen,[†] Kai Cui,[†] Songrui Zhao,[†] Dongping Liu,[‡] Hong Guo,[‡] Michel L. Trudeau,[§] Suzanne Paradis,[⊥] Abou-Rachid Hakima,[⊥] and Zetian Mi[†,*]

[†]Department of Electrical and Computer Engineering, McGill University, 3480 University Street, Montreal, Québec H3A 0E9, Canada, [‡]Centre for the Physics of Materials, Department of Physics, McGill University, 3600 University Street, Montreal, Québec H3A 2T8, Canada, [§]Science des Matériaux, IREQ, Hydro-Québec, 1800 Boulevard Lionel-Boulet, Varennes, Québec J3X 1S1, Canada, and [⊥]Defence Research and Development Canada Defence Valcartier, 2459 Boulevard Pie XI North, Québec, Québec G3J 1X5, Canada

ABSTRACT

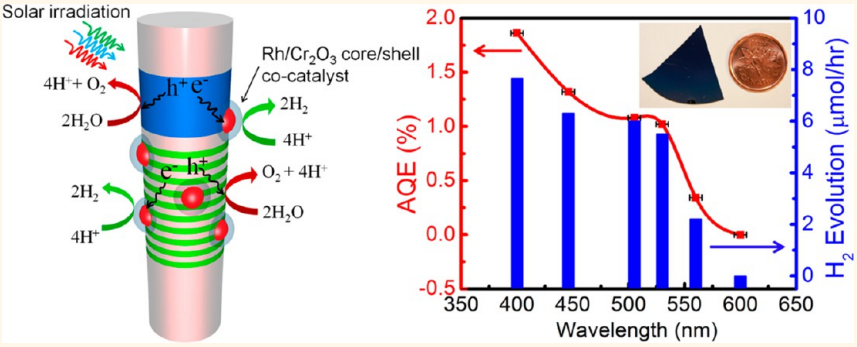

The conversion of solar energy into hydrogen *via* water splitting process is one of the key sustainable technologies for future clean, storable, and renewable source of energy. Therefore, development of visible light-responsive and efficient photocatalyst material has been of immense interest, but with limited success. Here, we show that overall water splitting under visible-light irradiation can be achieved using a single photocatalyst material. Multiband InGaN/GaN nanowire heterostructures, decorated with rhodium (Rh)/chromium-oxide (Cr_2O_3) core−shell nanoparticles can lead to stable hydrogen production from pure (pH ∼ 7.0) water splitting under ultraviolet, blue and green-light irradiation (up to ∼560 nm), the longest wavelength ever reported. At ∼440−450 nm wavelengths, the internal quantum efficiency is estimated to be ∼13%, the highest value reported in the visible spectrum. The turnover number under visible light well exceeds 73 in 12 h. Detailed analysis further confirms the stable photocatalytic activity of the nanowire heterostructures. This work establishes the use of metal-nitrides as viable photocatalyst for solar-powered artificial photosynthesis for the production of hydrogen and other solar fuels.

KEYWORDS: InGaN · GaN · nanowire · water splitting · hydrogen · photocatalytic · molecular beam epitaxy

Since the pioneering work by Fujishima and Honda,[1] photocatalytic water splitting has attracted considerable attention,[2,3] as it converts solar energy directly into hydrogen, a carbon-free, affordable and sustainable source of energy. Over the last 40 years, researches have been largely focused upon metal-oxide based photocatalyst materials[4,5] that are responsive to ultraviolet (UV) light (∼ 4% in solar spectrum). Success in finding abundant visible-light (∼43% in solar spectrum) active material, however, has been very limited.[6] This is attributed to the lack of known single photocatalyst material (one-step system) which has (i) sufficiently narrow bandgap (<3 eV) to harness visible photons, (ii) suitable band-edge potentials for overall water splitting (*i.e.*, simultaneous production of H_2 and O_2), and (iii) a high level of stability

* Address correspondence to zetian.mi@mcgill.ca.

Received for review June 7, 2013 and accepted August 12, 2013.

Published online August 12, 2013
10.1021/nn4028823

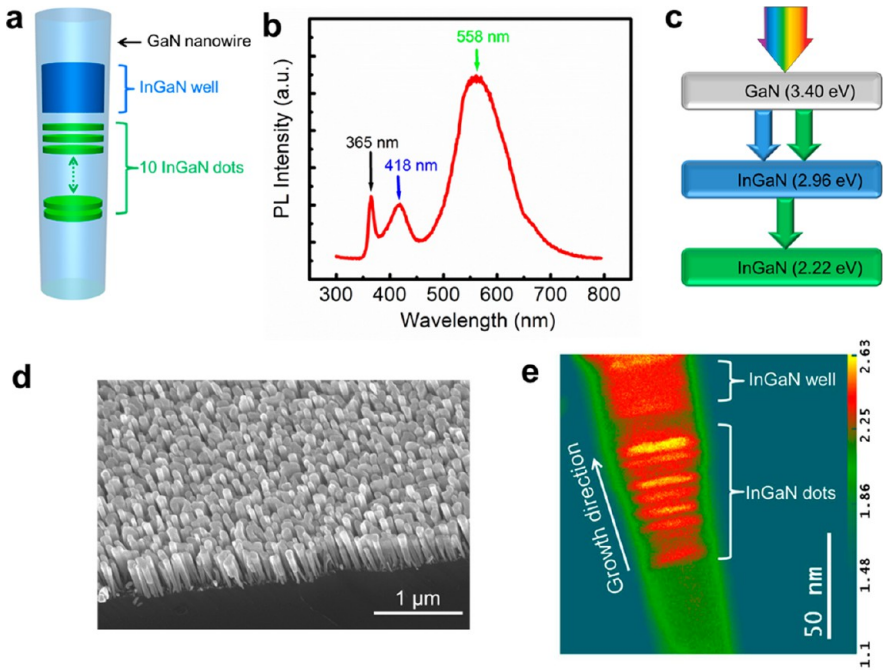

Figure 1. Growth and characterization of InGaN/GaN nanowire heterostructure. (a) Schematic of the InGaN/GaN nanowire heterostructure. (b) Room temperature photoluminescence spectra of InGaN/GaN nanowire arrays. (c) Schematic of InGaN/GaN triple-band nanowire heterostructure. (d) A 45° tilted SEM image of GaN/InGaN nanowire heterostructures grown on GaN nanowire templates on Si(111) substrate. (e) High angle annular dark field (HAADF) image in pseudocolor display of an as-grown InGaN/GaN nanowire heterostructure, showing the atomic number contrast between InGaN (red) and GaN (green) layers. The unit of intensity scale is 10^4 counts.

against photocorrosion.[6] In this regard, various energy-band engineering methods have been explored to transform UV-active materials into visible-light active photocatalyst but with limited success.[7−12] To date, most of these approaches cannot drive stable overall pure water splitting beyond the blue wavelength range.[8,13]

Here, we have developed a fundamentally different approach, with the use of multiband metal-nitride nanowire arrays, for achieving high-efficiency one-step hydrogen production from overall pure water splitting under visible-light irradiation. Compared to conventional oxide-based catalyst, the direct energy bandgap (E_g) of metal-nitrides, *e.g.*, InGaN, can be tuned to encompass nearly the entire solar spectrum.[14] Moreover, recent density functional theory (DFT) calculations showed that the band-edge potentials of InGaN can straddle the H^+/H_2 and O_2/H_2O redox potentials for indium compositions up to ∼50% (E_g ∼ 1.7 eV), thereby promising overall water splitting under the entire visible spectral range.[15] The large surface-to-volume ratios of nearly defect-free one-dimensional nanowires can further enhance the charge carrier separation, surface reaction rate and therefore the overall photocatalytic activity.[16,17] In addition, a multi-bandgap nanowire heterostructure facilitates efficient matching and utilization of incident solar irradiation.

In this study, catalyst-free InGaN/GaN multiband nanowire heterostructures were grown by radio frequency plasma-assisted molecular beam epitaxy (see Molecular Beam Epitaxial Growth). Vertically aligned GaN nanowire templates were first formed on Si(111) substrate under nitrogen-rich conditions. As schematically shown in Figure 1a, 10 self-organized InGaN/GaN quantum dots were subsequently incorporated along the axial dimension of the GaN nanowires. The dot heights are ∼3 nm, and indium compositions of the dots are varied in the range of ∼15−50% to effectively cover a broad absorption wavelength range. Such unique InGaN/GaN dot-in-a-wire nanoscale heterostructures enable the harness of sunlight in the green spectral range, without the formation of extended defects and dislocations resulting from the large lattice mismatch (∼11%) between InN and GaN.[18] To further enhance optical absorption in the blue wavelength range, an InGaN nanowire segment of ∼30 nm height and average indium composition of ∼11% was incorporated in the GaN nanowire, shown in Figure 1a, which is separated from the InGaN quantum dots by ∼15 nm GaN layer. The top GaN nanowire segment is p-doped using Mg, which may lead to enhanced photocatalytic activity for GaN under ultraviolet-light irradiation.[20]

The photoluminescence (PL) spectrum of InGaN/GaN nanowire heterostructures, shown in Figure 1b, was measured at room temperature (see Photoluminescence Measurement). It clearly shows the optical emission from GaN nanowire, InGaN ternary wire, and InGaN/GaN dot-in-a-wire structures, with the corresponding peak wavelengths at ∼365, ∼418, and ∼558 nm,

respectively. UV−visible diffuse reflectance spectroscopy (DRS) studies further demonstrate optical absorption by the GaN, InGaN well and InGaN dots (see Figure S1 in the Supporting Information).The average indium compositions for the InGaN ternary wire and InGaN dots were estimated to be ∼11% and ∼32%, respectively.[19] As illustrated in Figure 1c, the resulting InGaN/GaN nanowire heterostructure can function effectively as a triple-band structure for harvesting sunlight in the UV, blue, and green spectral range. The band-edge positions[15] of GaN, $In_{0.11}Ga_{0.89}N$ and $In_{0.32}Ga_{0.68}N$, with respect to water redox potential, is illustrated in Figure S2. As shown, both GaN and InGaN segments have sufficient overpotential for oxidation and reduction of water. Figure S3 is the band-diagram of InGaN/GaN nanowire heterostructure. Due to the presence of conduction and valence band offsets at the Si/GaN interface, the photoexcited carriers in Si substrate cannot migrate to GaN nanowire and hence do not take part in the water splitting reaction.

RESULTS AND DISCUSSION

Shown in Figure 1d is a 45° tilted scanning electron microscopy image of the as-grown InGaN/GaN nanowire ensemble on Si(111) substrate. The nanowires are vertically aligned to the substrate with nearly uniform height of ∼500 nm and lateral sizes of ∼30−70 nm, and the areal density is in the range of ∼1.5 × 10^{10} cm^{-2}. Structural properties of InGaN/GaN nanowire heterostructures were further studied using scanning transmission electron microscopy (STEM) and spectrum imaging. A high-angle annular dark field (HAADF) image of an InGaN/GaN nanowire in a pseudocolor display is shown in Figure 1e, illustrating the atomic number contrast between InGaN (red) and GaN (green). It is seen that 10 InGaN/GaN quantum dots are vertically aligned along the growth direction of the wire. The InGaN nanowire segment can also be identified.

Recent studies[20−22] confirmed that the GaN surface possesses adequate thermodynamic and kinetic potential for overall water splitting. To further verify that InGaN possesses the required potential for overall water splitting, as predicted by DFT calculations,[15] half reactions for individual evolution of H_2 and O_2 were first performed under visible-light illumination. A long-pass (λ > 385 nm) filter was utilized to optically excite only the InGaN material. CH_3OH (10 vol %) and $AgNO_3$ (0.1 M) were used as sacrificial reagents for H_2 and O_2 half reactions, respectively. Additionally, Pt (1 wt %) nanoparticles were *in situ* photodeposited from an aqueous H_2PtCl_6 solution to accelerate H_2O reduction reaction by introducing active reaction sites for gas evolution. In the case of H_2 half reaction, CH_3OH is oxidized by the photogenerated holes in the valence band, and therefore, the electrons can easily migrate to the surface of the photocatalyst where the H^+ ions

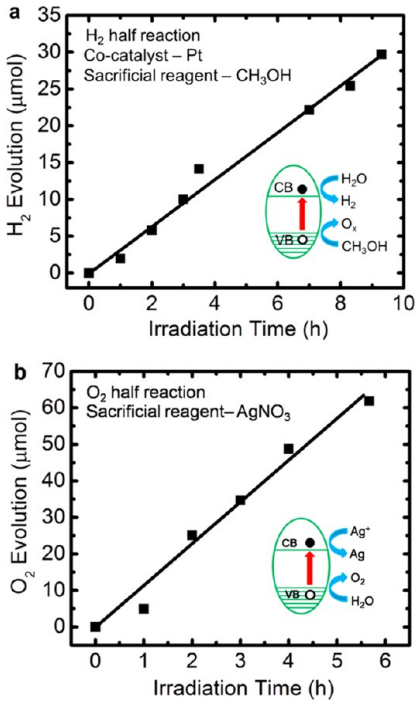

Figure 2. H_2 and O_2 half reactions under visible light. A long-pass (λ > 385 nm) filter was utilized to optically excite only the InGaN material. (a) Evolution of H_2 from half reaction in the presence of CH_3OH and Pt. (b) Evolution of O_2 from half reaction in the presence of $AgNO_3$. The insets illustrate the reaction mechanism. The solid line is a guide to the eye.

reduce to H_2. In O_2 half reaction, the photogenerated electrons in the conduction band reduce Ag^+ to Ag, while the valence band holes oxidize H_2O to O_2. The evolution of H_2 and O_2 exhibits a nearly linear increase over time, shown in Figure 2, panels a and b, respectively. Over ∼3 μmol/h of H_2 and ∼10 μmol/h of O_2 were produced during the course of the experiment, which confirmed that the conduction and valence band edge potentials of the present $In_xGa_{1-x}N$ nanowires meet the thermodynamic and kinetic requirements for H_2 and O_2 evolution. Controlled experiments further confirm that Pt nanoparticles can enhance the photocatalytic activity of our nanowire photocatalyst by nearly 20 times in the presence of sacrificial reagents (in half reaction).

In addition to the thermodynamic and kinetic potential requirement, the efficiency of photocatalytic water splitting is strongly influenced by surface electronic structure and charge properties. Because of the presence of an upward band-bending on the surfaces of nominally undoped or n-type Ga(In)N,[23] a tunneling-barrier is formed which can result in significant reduction of electron transfer to the surface reaction sites, and hence limit the H_2 production efficiency. A recent study[24] suggests that rhodium (Rh)/chromium-oxide (Cr_2O_3) core−shell nanoparticles can act as excellent H_2O reduction co-catalyst for H_2 evolution. In this regard, we have investigated the photodeposition

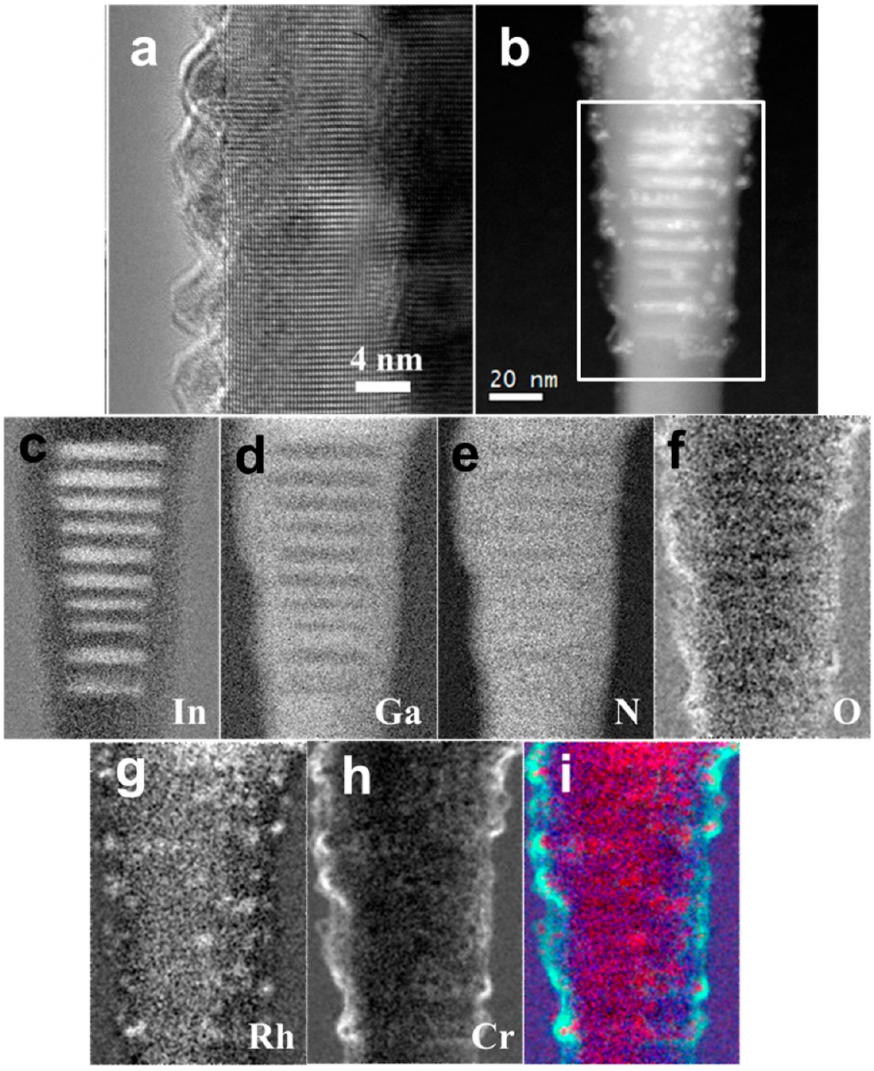

Figure 3. TEM characterization of Rh/Cr_2O_3 decorated InGaN/GaN nanowires. (a) High resolution TEM of Rh/Cr_2O_3 nanoparticles on the lateral surfaces of nanowire. (b) Electron energy loss spectroscopy (EELS) spectrum image of Rh/Cr_2O_3 deposited InGaN/GaN nanowire. (c−h) Elemental maps of the nanoparticle deposited InGaN/GaN nanowire, derived from the selected area in EELS spectrum image (b) with MLLS fitting. (i) RGB elemental mixing (red, Rh; green, Cr; blue, O) image showing the core−shell Rh/Cr_2O_3.

(see Photodeposition of Rh/Cr_2O_3 Core−Shell Nanoparticles) of Rh/Cr_2O_3 nanoparticles on the InGaN/GaN nanowire heterostructure. While Rh metal-core nanoparticle enhances the forward reaction of H_2O reduction, the Cr_2O_3 amorphous-shell suppresses the backward reaction to form H_2O from H_2 and O_2 on Rh core. Figure 3a shows a high resolution TEM (HRTEM) image of InGaN/GaN nanowires after photodeposition of Rh/Cr_2O_3 nanoparticles. The structural characterization (see Transmission Electron Microscopy) demonstrates that nanoparticles were deposited on the lateral surfaces of the crystalline nanowires. Additionally, an electron energy loss spectrometry (EELS) spectrum image (Figure 3b) confirms that the Rh/Cr_2O_3 nanoparticles formed a core/shell nanostructure on the nanowire surface. Because of the edge-overlap, the elemental distribution of In, Ga, N, O, Rh and Cr (Figure 2c−h) in the nanowire photocatalyst was derived from the EELS spectrum image (Figure 3b) with multiple linear least-squares (MLLS) fitting.[25] Our study reveals that the crystalline Rh nanoparticles are of ∼5 nm, which are covered by ∼2−3 nm thick amorphous Cr_2O_3 shell.[20] The Rh/Cr_2O_3 core−shell nanostructures are also clearly illustrated in the RGB image with Rh, Cr and O signal overlaid, shown in Figure 3i. X-ray photoelectron spectroscopy (XPS) analysis further confirms that the photodeposited nanoparticles consist of metallic Rh, mixed Rh−Cr oxide, and Cr_2O_3 (see X-ray Photoelectron Spectroscopy (XPS), Supporting Information and Figure S4).

In the subsequent photocatalytic overall pure water splitting experiments, ∼3.3 cm^2 substrate was used under a 300 W full arc (>300 nm) Xenon lamp. Considering the heights of ∼440 and ∼60 nm for GaN nanowire and InGaN nanowire segments, the corresponding material volumes are ∼4.0 and ∼0.38 μmol

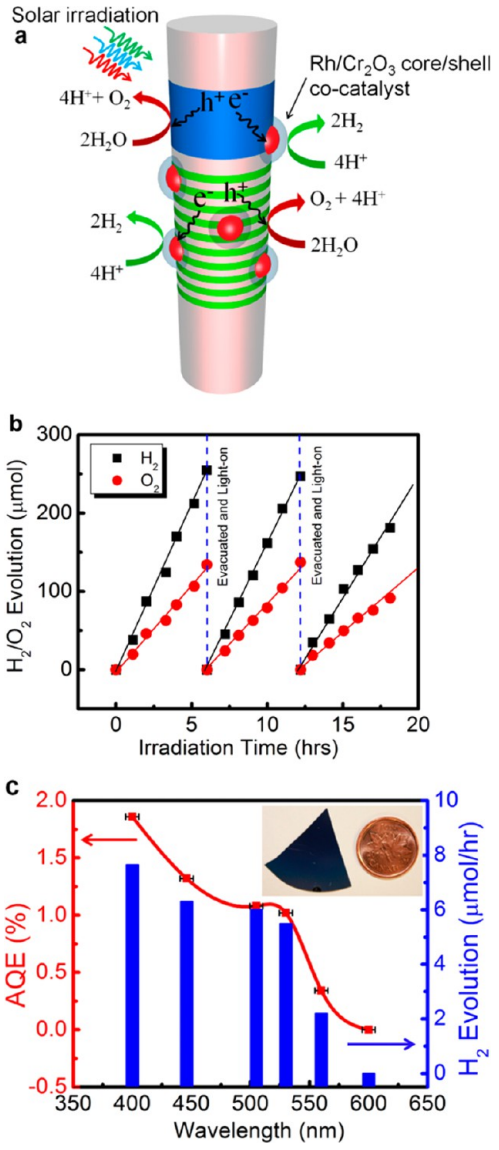

Figure 4. Overall water splitting and apparent quantum efficiency. (a) Schematic of the photocatalytic overall water splitting reaction mechanism. (b) Overall pure water splitting on Rh/Cr_2O_3 decorated InGaN/GaN nanowire arrays under full arc (>300 nm) 300 W xenon lamp irradiation. (c) Apparent quantum efficiency (AQE) (red line and solid square symbol, left axis) and H_2 evolution rate (blue columns, right axis) as a function of wavelength of the incident light. The horizontal error bars represent the full-width-half-maximum of the optical filters. The H_2 evolution rate was derived from ~2 h of overall water splitting under each optical filter. The solid red line is a guide to the eye. The inset shows a typical nanowire sample used for overall water splitting.

for GaN and InGaN, respectively. Figure 4a shows a schematic of the reaction mechanism on the Rh/Cr_2O_3 core−shell nanoparticle-decorated InGaN/GaN nanowire heterostructure. As illustrated, redox reaction of water occurs on both GaN nanowire and InGaN nanowire segments. For the production of molecular H_2 and O_2, four photons are simultaneously consumed to generate four holes (h^+) and electrons (e^-), which can catalyze water oxidation ($2H_2O + 4h^+ \rightarrow 4H^+ + O_2$) and proton reduction ($4e^- + 4H^+ \rightarrow 2H_2$) in overall water splitting, respectively. Figure 4b shows the overall pure water (pH ~ 7.0) splitting on Rh/Cr_2O_3 photodeposited InGaN/GaN nanowire heterostructures under full arc (>300 nm) irradiation. Stoichiometric evolution of H_2 and O_2 was evident in the absence of any sacrificial reagents. More than 1056 μmol gases evolved (~683 μmol of H_2 and ~373 μmol of O_2) during the course of ~18 h of experiment, which is substantially greater than the total amount of GaN and InGaN catalyst (~4.38 μmol) used in this experiment, suggesting that the reaction proceeded catalytically. The water splitting activity of the InGaN/GaN nanowire photocatalyst is further confirmed by adopting an AM1.5G filter. The photocatalytic activity with AM1.5G filter is 1.8 times lower than that under full arc illumination. The pH of water was invariant after the experiment, further indicating a balanced oxidation and reduction reaction of H_2O. The turnover number (defined as the ratio of total amount of H_2 evolved to the amount of catalyst) exceeded 155 after ~18 h of experiment under full arc (>300 nm) irradiation. The H_2 production rate is further calculated to be ~92 mmol h^{-1} g^{-1} of photocatalysts, which is nearly an order of magnitude higher than any previously reported photocatalyst for overall water splitting under full-arc irradiation.[26] The measured overall reaction represents a collective effect from the redox reactions driven by the charge carriers in the GaN wire, InGaN ternary wire and InGaN quantum dots upon the absorption of photons in the UV and visible spectral range. To clarify the importance of Rh/Cr_2O_3 co-catalyst, photocatalytic performance of InGaN/GaN nanowires was compared with and without co-catalyst (see Figure S5). As can be seen, the use of Rh/Cr_2O_3 nanoparticle co-catalysts can enhance the photocatalytic activity of InGaN/GaN nanowire heterostructures by nearly an order of magnitude. This improved activity is attributed to the introduction of active reaction sites, suppression of charge carrier recombination, and enhancement in charge separation along the lateral dimension.

To further evaluate the photocatalytic activity under visible light and to derive the apparent quantum efficiency (AQE) of the InGaN nanowire photocatalyst, the hydrogen and oxygen evolution rates were measured as a function of wavelength by adopting several band-pass filters (see Photocatalytic Reaction and Quantum Efficiency Measurement). Steady evolution of H_2 and O_2 was clearly observed under blue and green light irradiation (400−560 nm), providing unambiguous evidence that $In_xGa_{1-x}N$, for indium compositions of ~32% or lower, possesses suitable band-alignment and bandgap for overall pure water splitting. For comparison, no hydrogen can be observed under visible-light irradiation using structures without the incorporation of InGaN. As illustrated in Figure 4c, both the hydrogen-evolution rate and AQE decrease

with increasing wavelength. The highest AQE (~1.86%) is achieved at ~395–405 nm, which consists of the contribution from InGaN ternary wire (PL peak ~418 nm) and 10 vertically aligned InGaN quantum dots (PL peak ~558 nm). The longest wavelength (~560 nm) under which overall water splitting is achieved is in agreement with the PL peak (~558 nm) of the InGaN/GaN dot-in-a-wire structures, further confirming the photocatalytic activity of such quantum-confined nanoscale heterostructures. A typical wafer sample is also shown in the inset of Figure 4c. The maximum internal quantum efficiency was estimated (see Photocatalytic Reaction and Quantum Efficiency Measurement) to be ~13% at ~440–450 nm, for an absorption coefficient of 4×10^4 cm^{-1} for InGaN with an average indium composition of ~32%[27] and a total dot layer thickness of ~30 nm. To our knowledge, this is the highest quantum efficiency reported in the visible wavelength range for overall pure water splitting.[28] The turnover number under visible light (defined as the ratio of total amount of H_2 evolved under 400–600 nm irradiation as shown in Figure 4c to the amount of InGaN catalyst) exceeded 73 after ~12 h of experiment.

These studies correlate well with the dynamics of water dissociation at the $(10\bar{1}0)$ terminated GaN surfaces. First principles molecular dynamic simulations in recent past have suggested that the GaN $(10\bar{1}0)$ surfaces are very reactive for spontaneous dissociation of the majority (~83%) of the water molecules, $H_2O \rightarrow H^+ + OH^-$, which is in direct contrast with the most studied photocatalyst, TiO_2.[29] In addition, the low effective free-energy barrier for proton diffusion on GaN $(10\bar{1}0)$ surface facilitates enhanced migration of protons from the O_2 evolution reaction sites to H_2 evolution sites, which can eventually lead to an increased H_2 evolution in the present heterogeneous Rh/Cr_2O_3 decorated InGaN/GaN nanowire photocatalyst. The achievement of overall pure water splitting under blue and green light irradiation is also partly attributed to the inherent polarization-induced electric field in metal-nitrides[30] and the resulting quantum confined stark effect,[31] that can effectively suppress the recombination of photogenerated electrons and holes, and promote the transfer of charge carriers to the semiconductor/water interface. In addition, the extremely low surface-recombination velocity of III-nitrides, compared to that of other semiconductors, can further reduce nonradiative surface recombination. It is also worthwhile mentioning that the diffusion of photoexcited charge carriers to the surface may be reduced by the presence of a thin (~2–3 nm) GaN layer at the nanowire surface (see Figure 1e), formed due to indium evaporation from the surface during the growth process, which may limit the overall water splitting reaction rate in the present InGaN/GaN nanowire heterostructure. Significantly improved photocatalytic activity is therefore expected by optimizing the growth of nearly homogeneous InGaN nanowires with controlled surface charge properties.

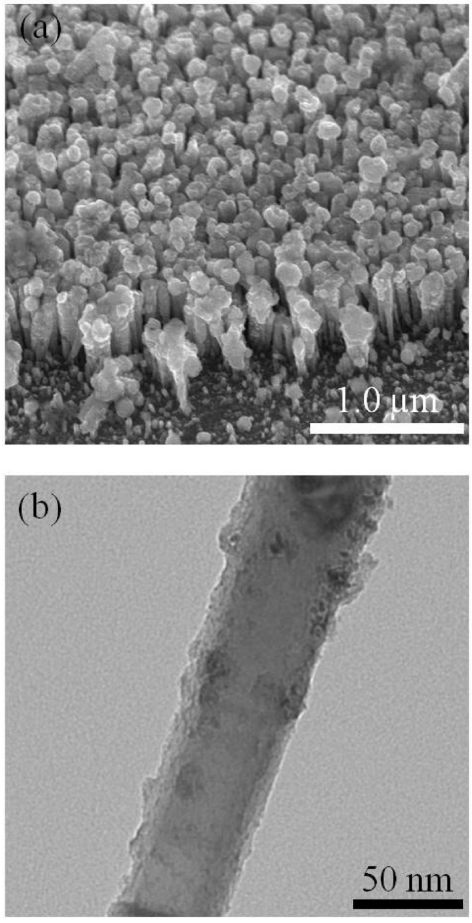

Figure 5. SEM and TEM characterization after overall water splitting. (a) SEM image of the InGaN/GaN nanowire ensemble after overall water splitting, showing the stability of the nanowire heterostructure. (b) Low magnification TEM image of a single InGaN/GaN nanowire after overall water splitting, further confirming the stability of the nanowire heterostructure.

The stability of the nanowire photocatalyst was further confirmed by detailed structural and surface analysis after the overall water splitting reaction. The SEM and TEM images of the InGaN/GaN nanowire heterostructure, taken after 18 h of water splitting reaction, are shown in Figures 5, panels a and b, respectively. No evidence of nanowire corrosion was found. These results further support the excellent chemical stability of III-nitride semiconductors in harsh photocatalytic reactions,[32] which is inherently related to the large difference in electronegativity between group III and group V elements.

CONCLUSION

In summary, we have demonstrated, for the first time, that InGaN, a widely used semiconductor for blue lasers, light emitting diodes, and power electronic devices, can function as a new material platform for

one-step, stable production of solar-fuels *via* photochemical water splitting under direct UV and visible light irradiation. Our work also shows that the use of nanowire structures allows for the design of multiband photocatalyst for efficient conversion of solar energy into clean fuels that was not previously possible by conventional photocatalysts, such as metal oxide powders. This wafer-level approach of water splitting offers recyclable and environmentally benign photocatalyst for large-scale practical applications.

METHODS

Molecular Beam Epitaxial Growth. In this study, vertically aligned InGaN/GaN nanowire heterostructures were grown on Si(111) substrate by radio frequency plasma-assisted MBE under nitrogen rich conditions without using any external catalyst. Instead of direct formation of InGaN nanowires on Si(111) substrate, a GaN nanowire template was used, which led to controlled formation of InGaN nanowires with excellent structural and optical properties. Each InGaN dot was capped by a ~3 nm thick GaN barrier layer. The growth parameters for GaN nanowire include a growth temperature of ~750 °C, nitrogen flow rate of 1.0 sccm, a forward plasma power of ~350 W, and a Ga beam equivalent pressure of $\sim 6 \times 10^{-8}$ Torr. To incorporate InGaN quantum dots, the growth temperature was reduced to ~600 °C. The composition and energy bandgap of InGaN ternary wires and quantum dots can be controlled by varying the In/Ga flux ratios and the growth temperature.

Photoluminescence Measurement. For the photoluminescence (PL) measurement of the nanowire heterostructure, a 266 nm diode-pumped solid state Q-switched laser was used as the excitation source. The emitted light was spectrally resolved by a high-resolution spectrometer, and detected by a photomultiplier tube.

Photodeposition of Rh/Cr_2O_3 Core−Shell Nanoparticles. The photodeposition of Rh/Cr_2O_3 core−shell nanoparticles was performed in two steps. For the first step, 2 μL of 0.2 mM sodium hexachlororhodate(III) (Na_3RhCl_6, Sigma Aldrich), 12 mL of CH_3OH, and 60 mL of Milli-Q water were placed in a 460 mL Pyrex chamber (Kimble Chase) with quartz lid. A homemade polytetrafluoroethylene (PTFE) holder was used to place the InGaN/GaN nanowire photocatalyst (on Si substrate) in the Pyrex chamber. Finally, the chamber was evacuated for 10 min, and subsequently irradiated using 300 W xenon lamp (PerkinElmer, PE300BF) for 15 min for photoassisted deposition of Rh nanoparticles. In the second step, the above-mentioned procedure was followed with 2 μL of 0.2 mM potassium chromate (K_2CrO_4, Sigma Aldrich) as a precursor for Cr_2O_3 deposition and the irradiation time was 30 min. The nanowire photocatalyst was then dried overnight in ambient.

Transmission Electron Microscopy. A CM200 microscope with an accelerating voltage of 200 kV was used to obtain bright-field transmission electron microscopy (TEM) images. For high-angle annular dark field (HAADF) imaging, energy dispersive X-ray spectrometry (EDXS) and electron energy loss spectroscopy (EELS) analysis, a FEI Titan 80-300 (scanning) transmission electron microscope ((S)TEM), operated at 300 kV and equipped with an aberration corrector of the probe-forming lens, and a high-brightness electron source were used. The electron beam diameter is approximately 0.2 nm. Also, in some cases, HAADF images were obtained using a Cs corrected Hitachi HD2700 dedicated STEM with a cold-field emitter-operated at 200 kV and having an electron beam diameter of approximately 0.1 nm.

X-ray Photoelectron Spectroscopy (XPS). The XPS system (Thermo Fisher Scientific K-Alpha) is equipped with a monochromatic Al−Kα X-ray source ($h\upsilon$ = 1486.6 eV), 180° double focusing hemispherical analyzer under an analysis chamber pressure of 10^{-8} Torr. The high resolution spectra were obtained using an X-ray beam size of 400 μm, pass energy of 50 eV, and a step size of 0.1 eV. The XPS results were evaluated using Avantage software (Thermo Scientific). Individual peak fitting was performed using convolution of Lorentzian and Gaussian line shapes (L/G = 30%). The binding energies were calibrated with Au $4f_{7/2}$ peak (84.0 eV) before each measurement.

Photocatalytic Reaction and Quantum Efficiency Measurement. The photocatalytic reactions were performed by adopting a 300 W xenon lamp (PerkinElmer, PE300BF) as an outer irradiation source and a Pyrex chamber with quartz lid, which allows ample transmission of both UV and visible-light irradiation. The chamber was evacuated prior to each experiment. The temperature of the reaction chamber was kept constant with a water bath. The reaction-evolved gases were sampled using a vacuum tight syringe and analyzed by a gas chromatograph (Shimadzu GC-8A) equipped with thermal conductivity detector (TCD) and high purity (99.99999%) Ar carrier gas. Because of manual sampling of the evolved gases, the experimental error in evolution measurement of H_2 and O_2 is estimated to be ~10%.

To derive the apparent quantum efficiency (AQE), several band-pass filters with center wavelengths of 400 nm (Newport: 20BPF10-400), 448 nm (Newport: 20BPF10-450), 502 nm (Newport: 20BPF10-500), 530 nm (Newport: 20BPF10-530), 560 nm (Newport: 20BPF10-560) and 600 nm (Newport: 20BPF10-600) were used. The transmission spectra of the band-pass filters are measured and shown in Figure S6, in order to confirm that there is no out-of-band transmission through the filters. The incident power density, measured using a calibrated Si photodetector (Newport: 818-ST-UV), varied between ~23 and 27 mW/cm^2 for wavelengths between 400 and 560 nm. The light reflections from the air/water and water/GaN interfaces were estimated to be ~14%, incorporating the refractive indexes of air, water, and GaN in calculations as 1.0, 1.33, and 2.3, respectively. The AQE was estimated from the following equation:[13]

$$\mathrm{AQE} = 2 \times \frac{\text{Number of evolved } H_2 \text{ molecules per hour}}{\text{Number of incident photons per hour}} \times 100\%$$

For deriving the internal quantum efficiency (IQE) at 440−450 nm, the absorbed photons were estimated based on the nanowire fill factor of ~70%, the total thickness of InGaN quantum dots (~30 nm) and the absorption coefficient of 4×10^4 cm^{-1} for InGaN with 32% indium composition.[27]

Conflict of Interest: The authors declare no competing financial interest.

Acknowledgment. This work was supported by the Natural Sciences and Engineering Research Council of Canada (NSERC) and Defence Research & Development Canada. Part of the work was performed in the Microfabrication Facility at McGill University. Electron microscopy images and analysis were carried out at the Canadian Centre for Electron Microscopy, a National facility supported by NSERC and McMaster University, and at IREQ, Hydro-Québec.

Supporting Information Available: XPS analysis of the cocatalyst, and stability of the Rh/Cr_2O_3 co-catalyst. This material is available free of charge *via* the Internet at http://pubs.acs.org.

REFERENCES AND NOTES

1. Fujishima, A.; Honda, K. Electrochemical Photolysis of Water at a Semiconductor Electrode. *Nature* **1972**, *238*, 37–38.
2. Tachibana, Y.; Vayssieres, L.; Durrant, J. R. Artificial Photosynthesis for Solar Water-Splitting. *Nat. Photonics* **2012**, *6*, 511–518.
3. Maeda, K.; Domen, K. Photocatalytic Water Splitting: Recent Progress and Future Challenges. *J. Phys. Chem. Lett.* **2010**, *1*, 2655–2661.

4. Kudo, A.; Miseki, Y. Heterogeneous Photocatalyst Materials for Water Splitting. *Chem. Soc. Rev.* **2009**, *38*, 253–278.
5. Guo, J., Chen, X. *Solar Hydrogen Generation: Transition Metal Oxides in Water Photoelectrolysis*; McGraw Hill: New York, 2012.
6. Maeda, K. Photocatalytic Water Splitting Using Semiconductor Particles: History and Recent Developments. *J. Photochem. Photobiology C: Photochem. Review* **2011**, *12*, 237.
7. Tong, H.; Ouyang, S.; Bi, Y.; Umezawa, N.; Oshikiri, M.; Ye, J. Nano-Photocatalytic Materials: Possibilities and Challenges. *Adv. Mater.* **2012**, *24*, 229–251.
8. Zou, Z.; Ye, J.; Sayama, K.; Arakawa, H. Direct Splitting of Water Under Visible Light Irradiation with an Oxide Semiconductor Photocatalyst. *Nature* **2001**, *414*, 625–627.
9. Asahi, R.; Morikawa, T.; Ohwaki, T.; Aoki, K.; Taga, Y. Visible-Light Photocatalysis in Nitrogen-Doped Titanium Oxides. *Science* **2001**, *293*, 269–271.
10. Khan, S. U. M.; Al-Shahry, M.; Ingler, W. B. Efficient Photochemical Water Splitting by a Chemically Modified n-TiO_2. *Science* **2002**, *297*, 2243–2245.
11. Maeda, K.; Takata, T.; Hara, M.; Saito, N.; Inoue, Y.; Kobayashi, H.; Domen, K. GaN:ZnO Solid Solution as a Photocatalyst for Visible-Light-Driven Overall Water Splitting. *J. Am. Chem. Soc.* **2005**, *127*, 8286–8287.
12. Chen, X.; Liu, L.; Yu, P. Y.; Mao, S. S. Increasing Solar Absorption for Photocatalysis with Black Hydrogenated Titanium Dioxide Nanocrystals. *Science* **2011**, *331*, 746–750.
13. Maeda, K.; Teramura, K.; Lu, D.; Takata, T.; Saito, N.; Inoue, Y.; Domen, K. Photocatalyst Releasing Hydrogen from Water. *Nature* **2006**, *440*, 295–295.
14. Wu, J. When Group-III Nitrides Go Infrared: New Properties and Perspectives. *J. Appl. Phys.* **2009**, *106*, 011101.
15. Moses, P. G.; Walle, C. G. V. d Band Bowing and Band Alignment in InGaN Alloys. *Appl. Phys. Lett.* **2010**, *96*, 021908.
16. Walter, M. G.; Warren, E. L.; McKone, J. R.; Boettcher, S. W.; Mi, Q.; Santori, E. A.; Lewis, N. S. Solar Water Splitting Cells. *Chem. Rev.* **2010**, *110*, 6446–6473.
17. Hwang, Y. J.; Wu, C. H.; Hahn, C.; Jeong, H. E.; Yang, P. Si/InGaN Core/Shell Hierarchical Nanowire Arrays and Their Photoelectrochemical Properties. *Nano Lett.* **2012**, *12*, 1678–1682.
18. Nguyen, H. P. T.; Zhang, S.; Cui, K.; Han, X.; Fathololoumi, S.; Couillard, M.; Botton, G. A.; Mi, Z. p-Type Modulation Doped InGaN/GaN Dot-in-a-Wire White-Light-Emitting Diodes Monolithically Grown on Si(111). *Nano Lett.* **2011**, *11*, 1919–1924.
19. Wu, J.; Walukiewicz, W.; Yu, K.; Ager, J. W.; Haller, E.; Lu, H.; Schaff, W. J. Small Band Gap Bowing in $In_{1-x}Ga_xN$ alloys. *Appl. Phys. Lett.* **2002**, *80*, 4741–4743.
20. Wang, D.; Pierre, A.; Kibria, M. G.; Cui, K.; Han, X.; Bevan, K. H.; Guo, H.; Paradis, S.; Hakima, A.-R.; Mi, Z. Wafer-Level Photocatalytic Water Splitting on GaN Nanowire Arrays Grown by Molecular Beam Epitaxy. *Nano Lett.* **2011**, *11*, 2353–2357.
21. Chen, P.-T.; Sun, C.-L.; Hayashi, M. First-Principles Calculations of Hydrogen Generation due to Water Splitting on Polar GaN Surfaces. *J. Phys. Chem. C* **2010**, *114*, 18228–18232.
22. Shen, X.; Small, Y. A.; Wang, J.; Allen, P. B.; Fernandez-Serra, M. V.; Hybertsen, M. S.; Muckerman, J. T. First-principles Calculations of Hydrogen Generation Due to Water Splitting on Polar GaN Surfaces. *J. Phys. Chem. C* **2010**, *114*, 13695–13704.
23. Bertelli, M.; Löptien, P.; Wenderoth, M.; Rizzi, A.; Ulbrich, R. G.; Righi, M. C.; Ferretti, A.; Martin-Samos, L.; Bertoni, C. M.; Catellani, A. Atomic and Electronic Structure of the Nonpolar GaN($1\bar{1}00$) Surface. *Phys. Rev. B* **2009**, *80*, 115324.
24. Maeda, K.; Sakamoto, N.; Ikeda, T.; Ohtsuka, H.; Xiong, A.; Lu, D.; Kanehara, M.; Teranishi, T.; Domen, K. Preparation of Core−Shell-Structured Nanoparticles (with a Noble-Metal or Metal Oxide Core and a Chromia Shell) and Their Application in Water Splitting by Means of Visible Light. *Chem.—Eur. J.* **2010**, *16*, 7750–7759.
25. Leapman, R. D.; Swyt, C. R. *Ultramicroscopy* **1988**, *26*, 393.
26. Maeda, K.; Teramura, K.; Saito, N.; Inoue, Y.; Domen, K. Domen, Improvement of Photocatalytic Activity of $(Ga_{1-x}Zn_x)(N_{1-x}Z_x)$ Solid Solution for Overall Water Splitting by Co-Loading Cr and Another Transition Metal. *J. Catal.* **2006**, *243*, 303–308.
27. Hahn, C.; Zhang, Z.; Fu, A.; Wu, C. H.; Hwang, Y. J.; Gargas, D. J.; Yang, P. Epitaxial Growth of InGaN Nanowire Arrays for Light Emitting Diodes. *ACS Nano* **2011**, *5*, 3970–3976.
28. Reece, S. Y.; Hamel, J. A.; Sung, K.; Jarvi, T. D.; Esswein, A. J.; Pijpers, J. J. H.; Nocera, D. G. Wireless Solar Water Splitting Using Silicon-Based Semiconductors and Earth-Abundant Catalysts. *Science* **2011**, *334*, 645–648.
29. Wang, J.; Pedroza, L. S.; Poissier, A.; Fernández-Serra, M. V. Water Dissociation at the GaN($10\bar{1}0$) Surface: Structure, Dynamics and Surface Acidity. *J. Phys. Chem. C* **2012**, *116*, 14382–14389.
30. Chichibu, S. F.; Abare, A. C.; Minsky, M. S.; Keller, S.; Fleischer, S. B.; Bowers, J. E.; Hu, E.; Mishra, U. K.; Coldren, L. A.; DenBaars, S. P.; *et al.* Effective Band Gap Inhomogeneity and Piezoelectric Field in InGaN/GaN Multiquantum Well Structures. *Appl. Phys. Lett.* **1998**, *73*, 2006–2008.
31. Lähnemann, J.; Brandt, O.; Pfüller, C.; Flissikowski, T.; Jahn, U.; Luna, E.; Hanke, M.; Knelangen, M.; Trampert, A.; Grahn, H. T. Coexistence of Quantum-Confined Stark Effect and Localized States in an InGaN/GaN Nanowire Heterostructure. *Phys. Rev. B* **2011**, *84*, 155303.
32. Li, J.; Lin, J. Y.; Jiang, H. X. Direct Hydrogen Gas Generation by using InGaN Epilayers as Working Electrodes. *Appl. Phys. Lett.* **2008**, *93*, 162107-1–162107−3.